Contents lists available at ScienceDirect

Journal of Wind Engineering and Industrial Aerodynamics

journal homepage: www.elsevier.com/locate/indaer

LES study on the turbulent flow fields over complex terrain covered by vegetation canopy

Zhenqing Liu [a], Takeshi Ishihara [b], Xuhui He [c,*], Huawei Niu [d]

[a] School of Civil Engineering and Mechanics, Huazhong University of Science & Technology, Wuhan, Hubei, China
[b] Department of Civil Engineering, School of Engineering, The University of Tokyo, Tokyo, Japan
[c] School of Civil Engineering, Central South University, Changsha, Hunan, China
[d] Department of Civil Engineering, Hunan University, Changsha, Hunan, China

ARTICLE INFO

ABSTRACT

In this study, (a) flat terrain covered by roughness blocks, (b) flat terrain covered by vegetation, (c) a 3-D hill covered by vegetation, and (d) a real forest covered complex terrain, were modeled step by step. For the flat terrain covered by roughness blocks, three different occupancy rates (25.0%, 12.5% and 5.6%) were examined. For each occupancy rate, three grid systems with different horizontal resolutions were examined. It was found that with intent to capture the turbulent characteristics accurately the horizontal grid size should be at least as large as the height of the roughness canopy. For the flow fields over vegetation covered flat terrain and a 3-D hill, the performance of the method modeling the vegetation used in this study was examined. The drag effects from the vegetation were modeled by adding a negative scour term in the momentum equation and satisfactory agreements with experiments were achieved. After sufficient validations, we reproduced the turbulent flow fields over a real forest covered complex terrain which is a terrain near Taikoyama hill, Kyoto, Japan, where extensive field measurements have been made available online by Kyoto Prefecture (2013). Two models for this real terrain with radius of the terrain equal to 4 km and 8 km in full scale were simulated under sixteen wind directions. Only the terrain model with large radius (8 km) gave good results. It is believed to be due to the factor that the model of small region terrain smoothed some upstream tall hills whose wake effects could be transported for a long distance downstream.

© 2016 Elsevier Ltd. All rights reserved.

1. Introduction

The accurate prediction of the wind energy distribution over terrains is important for making an appropriate selection of a suitable site when installing wind power plant, because wind energy production is proportional to the cubic of wind speed. The wind resource is rich in some mountainous regions, but the distribution of wind speed is very complex, therefore an accurate prediction of the wind speed and the turbulence statistics of the flow over curved topography is now becoming more and more important. Except for the wind turbine sitting, prediction of the turbulent flow fields over topography is also important for many other engineering applications, such as safety of structures, wind damage to agriculture, and aviation safety. In the case of flow over curved topography, the flow fields in the wake are very sensitive to the oncoming flow condition which affects the locations of the separation and reattachment points, making the study about this

kind of wake flow difficult. Moreover in the mountainous region the land is always covered by forest which will generate more turbulence and the significant effects from the forest to the mean flow could not be ignored, therefore the drag effects from the forest should also be taken into consideration. Numerical prediction of the effects of surface roughness on flow fields is one of the important areas within the wind engineering studies. In order to have an accurate prediction of flows over topographic features with the influence of ground roughness, the boundary conditions must be correctly selected.

Up to now there are two types of methods accounting for the ground roughness effects. One is to apply the logarithmic wall function to modify the wall stresses based on the roughness length, z_0, and the other one is to apply the canopy model which modifies the momentum equations by adding a drag term to account for the drag effects from the roughness.

The first approach, using logarithmic wall function, is widely adopted in the numerical studies about the flow over roughness covered topography, due to its convenience for application. Castro et al. (2003) applied two-equation k–ε turbulence model to study the flow over the Askervein Hill and they found that the flow's

* Corresponding author.
  E-mail address: xuhuihe@csu.edu.cn (X. He).

Nomenclature

$f_{\bar{u},i}$	source term for the ith momentum equation
l_0	representative length of canopy
γ_0	solid packing density of canopy
V_u	volume roughness blocks occupied
S_u	projective area of the solid
$C_{D,\bar{u}_i}$	drag force coefficient of the canopy
z_m	elevation of the modified terrain

h_r	Height of roughness canopy
U	mean streamwise velocity
V	mean spanwise velocity
W	mean vertical velocity
σ_u	wind fluctuation in streamwise direction
σ_v	wind fluctuation in spanwise direction
σ_w	wind fluctuation in s vertical direction
I_u	turbulence intensity
k	kinetic energy

---

most prominent feature was a recirculation region in the lee of the hill which could be fully captured only in the case of a time-dependent formulation and a third-order discretization of the adjective terms. Kim et al. (2000) applied the standard and RNG-based k–ε models to simulate the flow at four sites, Cooper's Ridge in New South Wales, Australia, Kettles Hill in Alberta, Canada, Askervein Hill in Scotland and Sirhowy Valley in South Wales. They found the RNG-based k–ε model gives better results than the standard k–ε model. Lun et al. (2003) studied the flow over two types of topographic features using three turbulence models i.e. standard k–ε model, Durbin model which is a linear revised k–ε model and Shin model which is a nonlinear revised k–ε model. In the wake of the hill the predictions by Shin model gives best performance. Diebold et al. (2013) applied immersed boundary method (IBM) together with the LES turbulence model to simulate the flow around steep terrain and found that the largest disagreement observed near the surface confirming the importance of using appropriate surface roughness. Lopes et al. (2007) examined the performance of RANS model and LES model for simulating the flow over real terrain. They concluded that in the upstream side of the hill, the large-eddy simulations predict the turbulent kinetic energy better than the RANS model. They also pointed out that the major problem is the prediction of separation related to the incorrect modeling of the decelerating boundary layer through logarithmic wall method.

The second approach, using canopy model, is now attracting more and more attentions of the researchers because of its ability of considering the drag effects from the roughness physically. In this model the equation of momentum for roughness are coupled with the Navier–Stokes equation so turbulence in the roughness canopy can be numerically expressed. Tamura et al. (2007) studied the effects of vegetation on turbulence statistics of the flow over a 3D steep hill through large eddy simulations. The high intensity due to the coherent flow structures at the top of the vegetation and reduction of turbulence inside the vegetation were clarified. Dupont et al. (2008) examined the turbulent flow within and above a forested canopy on an isolated two-dimensional hill and validated against pressure as well as velocity data from a wind-tunnel experiment. They concluded that the LES turbulence model together with the canopy model is able to accurately reproduce the main features observed over a forested hill. Cao et al. (2012) used roughness blocks arranged on a 2-D hill to simulate the rough condition and an immersed boundary method (IBM) was used to model roughness elements by adding an external force term in the volumes occupied by the blocks. This method is different with the studies by Tamura et al. (2007) and Dupont et al. (2008) because the added drag force term in those studies is to model each single solid roughness block. Cao et al. (2012) concluded that the generation of inflow turbulence and modeling the effects of roughness blocks play important roles in simulating the turbulent boundary layer over hills. Large-eddy simulation combined with the canopy model has been proved to be able to reproduce many features of turbulent flow over vegetation on flat

terrain or simplified topographies. However, the application of this technique to examine the flow over real complex terrain is lacked which is the motivation of the present study.

Apart from numerical approaches studying the flow fields over roughness covered complex topography, some experiments have also been carried out, such as Finnigan et al. (1990), Ishihara et al. (2001) and Yamaguchi et al. (2003), Cao and Tamura (2006, 2007). However, a complex terrain usually requires modeling of an area that is too large to achieve in a wind tunnel.

This research aims to adopt the LES turbulent model together with the canopy model to simulate the flow over forest covered real complex terrain. Four cases, (a) flat terrain covered by roughness blocks, (b) flat terrain covered by vegetation, (c) a 3-D hill covered by vegetation, and (d) a real forest covered complex terrain, were modeled.

- For the flat terrain covered by roughness blocks, three different occupancy rates are examined. And for each occupancy rate, three grid systems with different horizontal resolutions are checked. Quantitative guidelines determining the horizontal grid resolution when the canopy model is applied were provided.
- In the real complex terrain the land is always covered by trees, which is different with the canopy of roughness blocks, so we then checked the performance of the method used in this study by reproduction the flow fields over vegetation covered flat terrain and a 3-D hill. The numerical results were compared to experimental results from other research works in order the method to be validated.
- At last the turbulent flow fields over a real forest covered complex terrain, which is a terrain near Taikoyama hill, Kyoto, Japan, where extensive field measurements have been made available online by Kyoto Prefecture (2013), were simulated under sixteen wind directions. Two models with radius of the terrain equal to 4 km and 8 km in full scale were simulated to examine how large the radius of terrain is enough to provide accurate predictions.

2. Numerical model and boundary condition

The governing equations are introduced in Section 2.1. Sections 2.2 and 2.3 present the method modeling roughness blocks and the vegetation canopy. Section 2.4 gives the information of the solution scheme and the solution procedure.

2.1. Governing equations

Momentum and mass are primarily transported by large eddies; therefore, large-eddy simulation (LES) is adopted. In such simulations, large eddies are directly computed, while the influence of eddies smaller than grid spacing are parameterized. The Boussinesq hypothesis is employed, and the standard

Smagorinsky–Lilly model is used to calculate the subgrid-scale (SGS) stresses.

The governing equations are obtained by filtering the time-dependent Navier–Stokes equations in Cartesian coordinates (x, y, z), which can be expressed as follows:

$$\frac{\partial \rho \tilde{u}_i}{\partial x_i} = 0 \tag{1}$$

$$\rho \frac{\partial \tilde{u}_i}{\partial t} + \rho \frac{\partial \tilde{u}_i \tilde{u}_j}{\partial x_j} = \frac{\partial}{\partial x_j}\left(\mu \frac{\partial \tilde{u}_i}{\partial x_j}\right) - \frac{\partial \tilde{p}}{\partial x_i} - \frac{\partial \tau_{ij}}{\partial x_j} \tag{2}$$

where x_i (x: streamwise, y: spanwise, z: vertical) are the co-ordinates, $\tilde{u}_i$ and $\tilde{p}$ are the filtered velocities and pressure, respectively, μ is the viscosity, ρ is the density, and τ_{ij} is the SGS stress, which is modeled as follows:

$$\tau_{ij} = -2\mu_t \tilde{S}_{ij} + \frac{1}{3}\tau_{kk}\delta_{ij}; \quad \tilde{S}_{ij} = \frac{1}{2}\left(\frac{\partial \tilde{u}_i}{\partial x_j} + \frac{\partial \tilde{u}_j}{\partial x_i}\right) \tag{3}$$

where μ_t denotes the SGS turbulent viscosity, $\tilde{S}_{ij}$ is the rate-of-strain tensor for the resolved scale, and δ_{ij} is the Kronecker delta. The Smagorinsky–Lilly model is used for the SGS turbulent viscosity

$$\mu_i = \rho L_s^2 |\tilde{S}| = \rho L_s \sqrt{2\tilde{S}_{ij}\tilde{S}_{ij}}; \quad L_s = \min\left(\kappa d, C_s V^{1/3}\right) \tag{4}$$

in which L_s denotes the mixing length for subgrid-scales, κ is the von Kármán constant, i.e., 0.42, d is the distance to the closest wall and V is the volume of a computational cell. In this study, C_s is Smagorinsky constant, which is determined to be 0.1 for the atmospheric boundary layer (ABL) flow same as the study by Liu et al. (2016).

When the wall-adjacent cells are in the laminar sublayer, the wall shear stresses are obtained from the laminar stress–strain relationship

$$\frac{\tilde{u}}{u_\tau} = \frac{\rho u_\tau y}{\mu} \tag{5}$$

If the mesh cannot resolve the laminar sublayer, it is assumed that the centroid of the wall-adjacent cells falls within the logarithmic region of the boundary layer, and the law-of-the-wall is employed as follows:

$$\frac{\tilde{u}}{u_\tau} = \frac{1}{\kappa}\ln E\left(\frac{\rho u_\tau y}{\mu}\right) \tag{6}$$

where $\tilde{u}$ is the filtered velocity tangential to wall, y is the distance between the center of the cell and the wall, u_τ is the friction velocity, and the constant E is 9.793.

In the present study we mainly examine flow fields over the terrain covered by roughness. In order to consider drag effects from roughness, canopy model is used, in which the roughness is not directly resolved whereas drag forces are added into the momentum equations to reproduce their aerodynamic drag effects. The governing equations in the roughness canopy are

$$\rho \frac{\partial \tilde{u}_i}{\partial t} + \rho \frac{\partial \tilde{u}_i \tilde{u}_j}{\partial x_j} = \frac{\partial}{\partial x_j}\left(\mu \frac{\partial \tilde{u}_i}{\partial x_j}\right) - \frac{\partial \tilde{p}}{\partial x_i} - \frac{\partial \tau_{ij}}{\partial x_j} + f_{\bar{u},i} \tag{7}$$

where $f_{\bar{u},i}$ is the source term for the ith momentum equation and can be determined following the study by Enoki and Ishihara (2012) for different types of roughness as will be reviewed below.

2.2. Modeling roughness block

For the roughness blocks, the drag force terms added in the

momentum equation is determined as

$$f_{\bar{u},i} = -\frac{1}{2}\rho C_{f_i}\frac{\gamma_0}{l_0}\tilde{u}_{mag}\tilde{u}_i \tag{8}$$

where C_{f_i} is the drag coefficient in i direction, l_0 is the representative length and γ_0 is the physical defined solid packing density, and $\tilde{u}_{mag}$ is the magnitude of fluid speed. The representative length and the solid packing density are

$$\gamma_0 = \frac{V_u}{V_{grid}} \quad \text{and} \quad l_0 = \frac{V_u}{S_u/4} \tag{9}$$

where V_{grid} is the computational grid volume in which the solid volume V_u is occupied and S_u is the projective area of the solid. The drag coefficient C_{fi} is calculated as the formulation proposed by Enoki and Ishihara (2012) through fitting the experimental data

$$C_{fi} = \frac{1}{(1-\gamma_0)^3}\min\left(\frac{1.53}{(1-\gamma_0)}, \ 2.75(1-\gamma_0)\right) \tag{10}$$

2.3. Modeling vegetation

For the vegetation, the drag force terms added in the momentum equation is determined as

$$f_{\bar{u},i} = \frac{1}{2}\rho C_f \frac{\gamma_0}{l_0}\tilde{u}_{mag}\tilde{u}_i \tag{11}$$

where $C_f = C_{D,\bar{u}_i}/\left(1-\gamma_0^2\right)$, $C_{D,\bar{u}_i}$ is the drag coefficient and determined as 0.4 following the suggestion from Kaimal and Finnigan (1994); γ_0 is the volume occupancy rate; and l_0 is the thickness of the leaf.

2.4. Solution scheme and solution procedure

The 3D unsteady LES filtered Navier–Stokes equations were solved with the commercial CFD code ANSYS/Fluent6.3 (Fluent Inc., 2006) using the control volume method. The second order central difference scheme was used for the convective and viscosity term, and the second order implicit scheme for the unsteady term. SIMPLE (semi-implicit pressure linked equations) algorithm was employed for solving the discretized equations (Ferziger and Peric, 2002). Time step size was 0.0001 s. For all of the simulations after 2 s the initial transient effects were found to disappear, in another words the flow reached a stable stage. The turbulent fields were averaged in time over 6×10^4 instantaneous samples and collected every time step during a 6 s period.

3. Numerical simulations

In this section four models, (a) flat terrain covered by roughness blocks, (b) flat terrain covered by vegetation canopy, (c) 3-D hill covered by vegetation canopy and (d) real complex terrain covered by forest, will be numerically simulated.

3.1. Flat terrain covered by roughness blocks

In this section we want to validate the canopy model for simulating the roughness blocks and also give suggestions determining the horizontal grid resolution when the canopy model is applied.

3.1.1. Simulation setup

In the experiment by Maruyama (1993) roughness blocks with occupancy rates, γ_0, of 5.6%, 12.5% and 25.0% were studied.
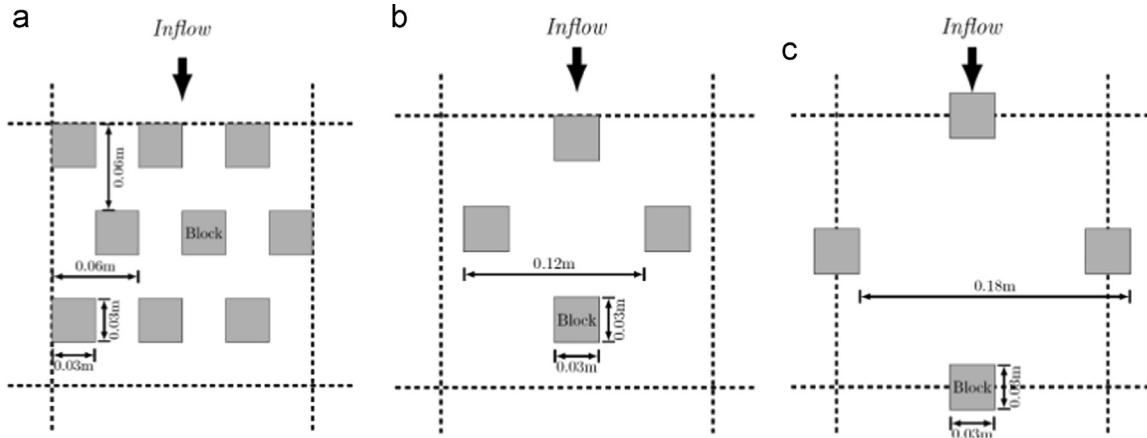
Fig. 1. Arrangement of roughness blocks with density of (a) 25.0%, (b) 12.5% and (c) 5.2%.
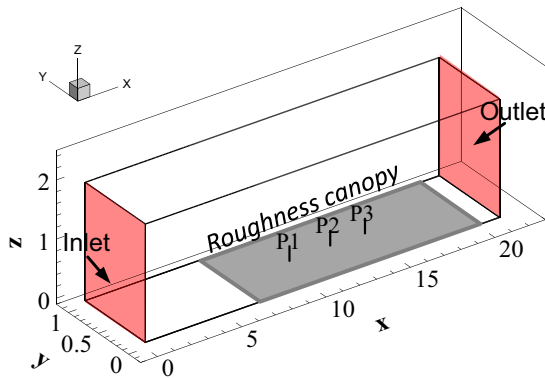
Fig. 2. Configuration of the numerical wind tunnel simulating the canopy of roughness blocks. Unit:meter.

Fig. 3. Vertical grid distribution of the numerical wind tunnel simulating the roughness blocks canopy (fine grid case).

Similarly to the experiment three kinds of homogeneous roughness, $\gamma_0 = 5.6\%$, $\gamma_0 = 12.5\%$ and $\gamma_0 = 25.0\%$ are examined numerically. The height of roughness blocks, h_r, is 0.03 m, as shown in Fig. 1 which is a repeating pattern throughout the roughness canopy area for all occupancy rates. The computational domain has a height of 2 m, length of 21 m. Mason and Thomson (1987) recommended a width of approximately 2 times the boundary layer depth as for reproducing the largest eddies in atmospheric boundary layer and from the experimental data by Maruyama (1993) the boundary layer depths are found to be less than 0.5 m for all of the three cases. As a result, 1.0 m is used for the width of the computational domain. The roughness canopy starts from 6.8 m and ends at 19.9 m. At the locations $x=8.11$ m (P1), $x=10.51$ m (P2) and $x=12.95$ m (P3) the mean wind speed and turbulent kinetic energy will be measured. The gray region in Fig. 2 illustrates the location covered by the roughness canopy. All the geometry parameters in the computational domain are same as those in the experiment except the width of the domain. The width is 0.82 m less than the wind tunnel used in the experiment, with the consideration of saving the computational resources. Canopy model was applied to model the roughness blocks. The source term in the momentum equation could be determined from Eq. (8). The length scale l_0 and the drag coefficient C_{fi} could be determined by Eqs. (9) and (10) respectively.

Numerical models with three horizontal (x–y plane) grid resolutions, 0.03 m (Fine), 0.06 m (Medium), and 0.12 m (Rough), were built. For the three grid systems, the vertical grid distributions are same. At the bottom and the top of the canopy region the vertical grid size is 0.0005 m. The maximum vertical grid size in canopy is 0.003 m and the number of grid along the height of
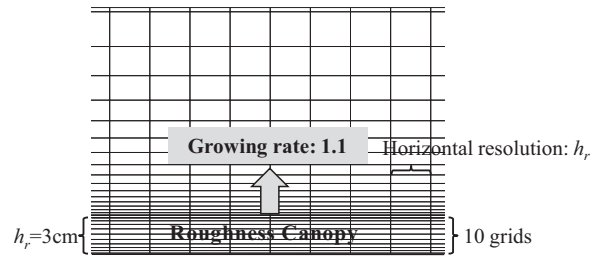
canopy is 10. Above the top of the canopy the grid starts from 0.0005 m and grows with a ratio of 1.1, as could be found in Fig. 3. The total grid number is 720,000 (Fine), 180,000 (Medium) and 45,000 (Rough).

As for boundary conditions, a stress-free condition ($\partial u/\partial n = 0$, $\partial v/\partial n = 0$, $w=0$) was used at the top of the domain and a symmetry condition ($\partial u/\partial n = 0$, $\partial w/\partial n = 0$, $v=0$) at the spanwise sides. Uniform wind flow with a speed of 1.0 m s^{-1} was set at the inlet ($p = 0$, $u=1.0$ m s^{-1}, $v=0$, $w=0$). At the end of the wind tunnel, outlet boundary condition ($\partial p/\partial n = 0$, $\partial u/\partial n = 0$, $\partial v/\partial n = 0$, $\partial w/\partial n = 0$) is applied. Non-slip condition ($u=0$, $v=0$, $w=0$, $\partial p/\partial n = 0$) was used at the bottom surface.

3.1.2. Numerical results

Fig. 4 shows the instantaneous flow fields visualized by vorticity of y component $\partial w/\partial x - \partial u/\partial z$. The turbulence statistics including the mean streamwise velocity, U, and the kinetic energy, k is shown in Fig. 5. The data used for the plotting of Figs. 4 and 5 are from the fine grid system. In the later discussion it will be found only the fine grid system could provide satisfactory results. It can clearly be found from Fig. 4 that even the roughness blocks are not directly built the turbulence flow could also be successfully generated if the canopy model is used. The turbulence develops as soon as the flow touches roughness blocks and the boundary layer thickness increases as the flow propagating as illustrated in Fig. 5.

The profiles of mean streamwise velocity, U, and the kinetic energy, k, at the measurement points P1, P2 and P3 obtained from fine, medium and coarse grid systems are plotted in Fig. 6, superimposed on which is the experimental data from Maruyama (1993) as illustrated by circles. It can be clearly seen that only the results from the fine horizontal resolution (3 cm $\times$ 3 cm), whose grid size on x–y plane is same as the height of the roughness blocks, show satisfactory agreement with the experimental results. The other two models (grid size on x–y plane: 6 cm $\times$ 6 cm and 12 cm $\times$ 12 cm) give large discrepancies with the experiment. It is
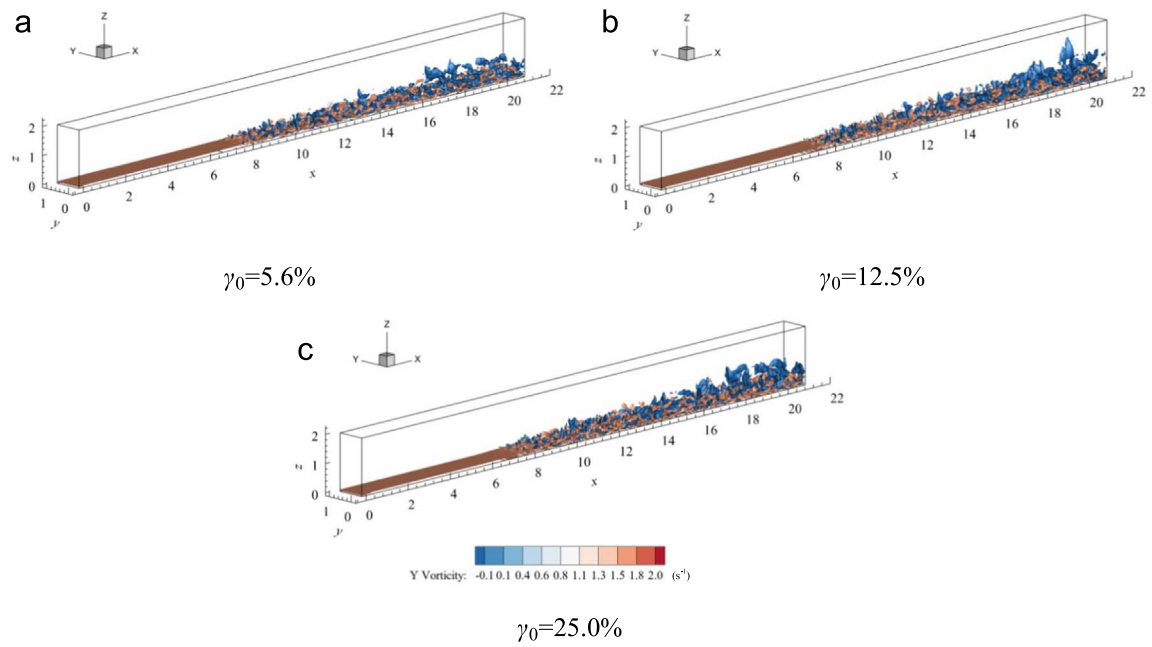
Fig. 4. Vorticity isosurfaces of the turbulent flow fields computated in fine grid system over roughness blocks with density of (a) 5.6%, (b) 12.5% and (c) 25%. Unit:meter.
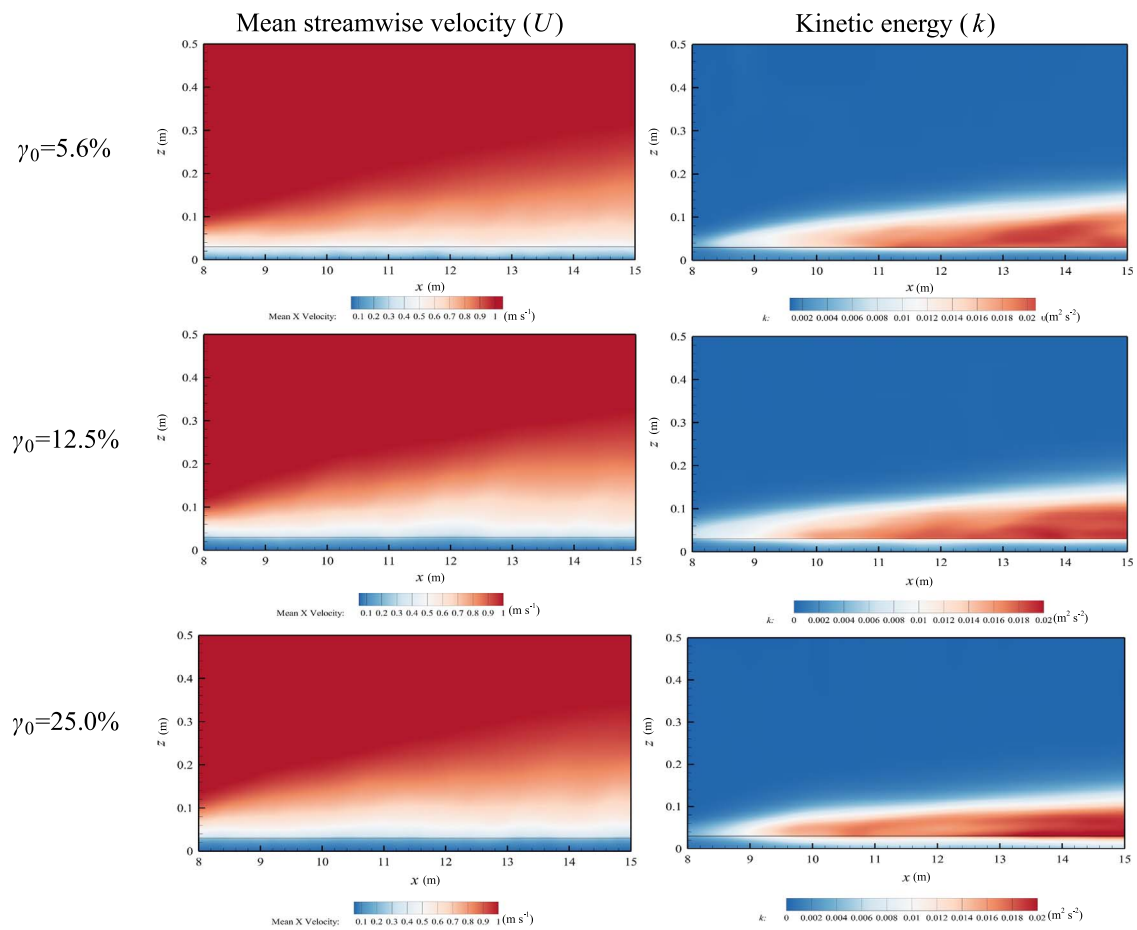
Fig. 5. Contour of mean streamwise velocity and kinetic energy of the flow over roughness blocks with density of 5.6%, 12.5% and 25% computated in fine grid system.

Mean streamwise velocity (U)   Kinetic energy (k)
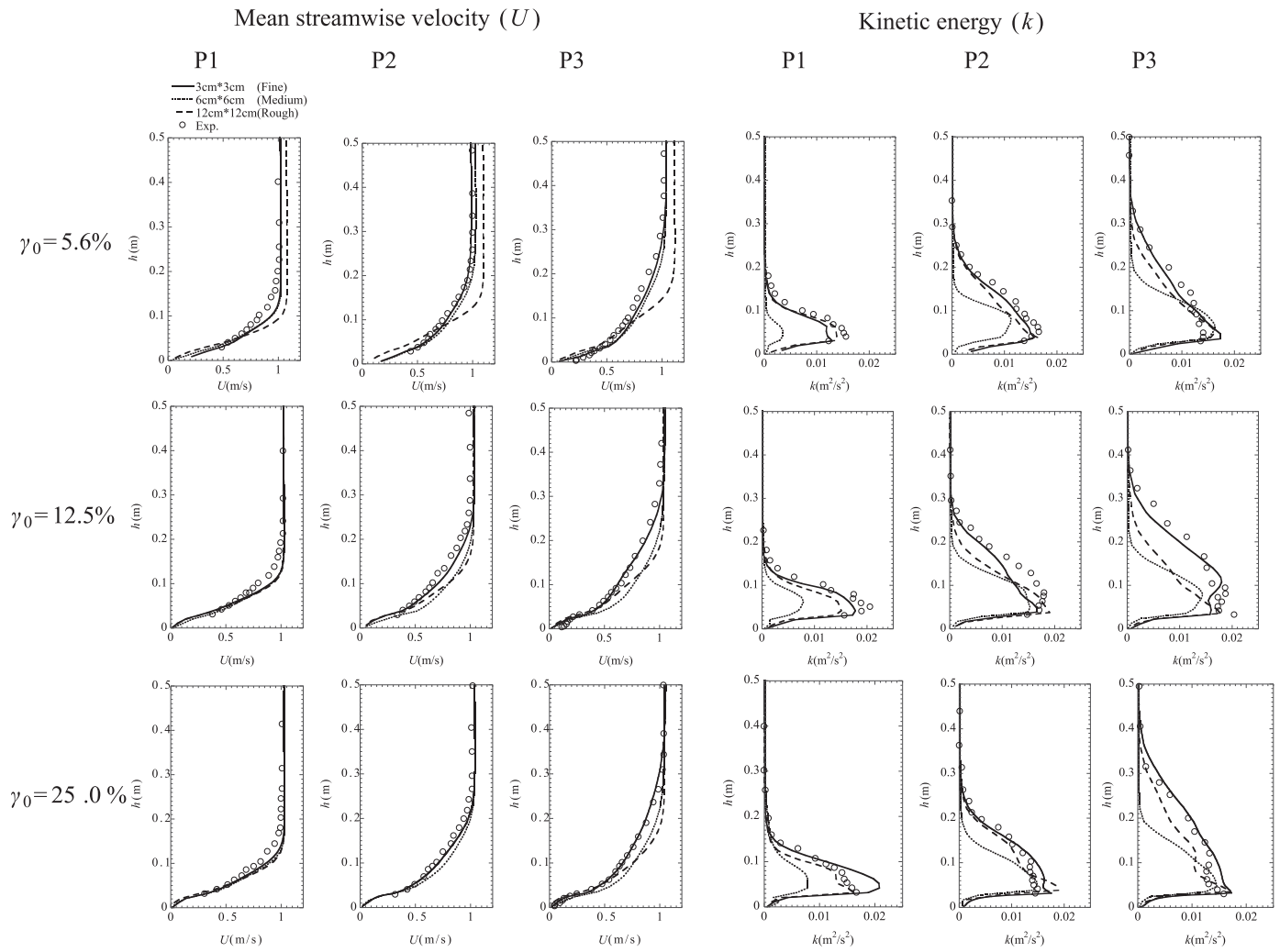
Fig. 6. Comparison of the profiles of mean streamwise velocity and kinetic energy of the flow roughness blocks with density of 5.6%, 12.5% and 25% from models with different horizontal resolutions and the experiments.

the indication that in order to reproduce flow fields over roughness by the canopy model the horizontal grid resolution should be at least same as the height of the roughness canopy when LES turbulent model is applied.

3.2. Flat terrain covered by vegetation canopy

In this section we want to validate this method modeling vegetation canopy through a simple flat terrain covered by grass in one wind tunnel experiment by Ishihara and Hibi (1998).

3.2.1. Simulation setup

In order to evaluate the method modeling vegetation canopy, data obtained from an experimental study by Ishihara and Hibi (1998) were used. In that experiment the artificial grass, whose volume occupancy rate γ_0 and the thickness of the leaf, l_0, were measured as 0.12 and 0.0013 m respectively. The experiment was conducted in a wind tunnel with a test section of 1.1 m wide, 0.9 m high and 7 m long. The neutrally stratified atmospheric boundary layer was simulated using 60mm high cubic elements followed by 20 mm and 10;mm cubic blocks covering 1.2 m of the test-section
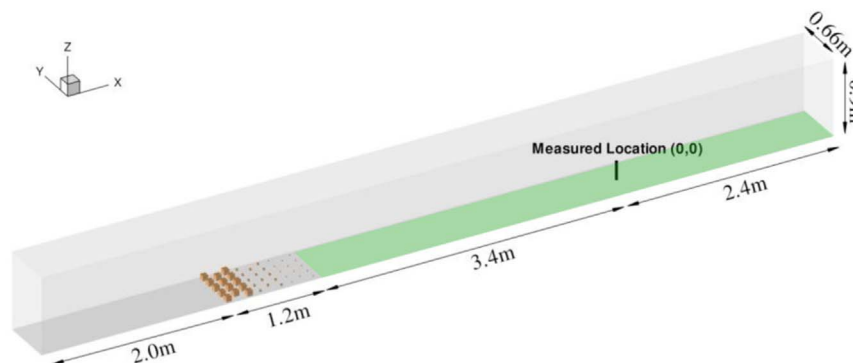
Fig. 7. Configuration of numerical model simulating flat terrain covered by vegetation canopy.
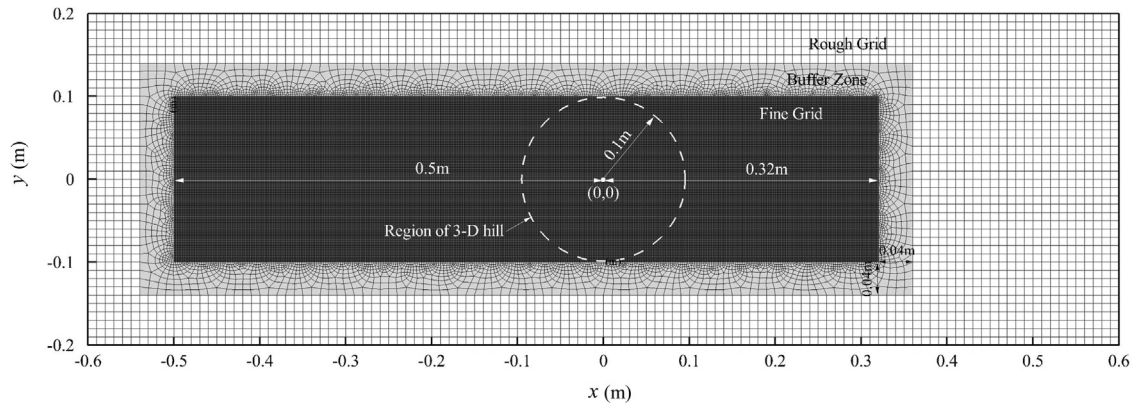
Fig. 8. Sketch map of the locations of the rough grid, buffer zone, and fine grid of the nested grid simulating flat terrain covered by vegetation canopy. White dashed line presents the region covered by a 3-D hill.

floor. Each group of the blocks has three rows and the roughness blocks cover a region with a length of 0.4 m in streamwise direction. The roughness blocks here are directly modeled by walls. The grass starts just after the roughness blocks and ends at the outlet of the wind tunnel. The height of grass is 5 mm. The configurations of the numerical wind tunnel are same as those in experiment except the width of the wind tunnel and the upstream buffer zone, see Fig. 7, where the origin point is 3.4 m downstream of the roughness blocks. Two times of the boundary layer thickness, 0.66 m, was determined as the width of wind tunnel based on the suggestions from Mason and Thomson (1987). The upstream buffer zone, 2.0 m long, was appended to avoid any perturbations from the inlet condition into the turbulence generation region. The outlet of the numerical wind tunnel was set at the location with a distance of 2.4 m from the origin point to avoid any influence from the outlet into the region of concern.

As boundary conditions, a stress-free condition ($\partial u/\partial n = 0$, $\partial v/\partial n = 0$, $w=0$) was used at the top of the domain and a symmetry condition ($\partial u/\partial n = 0$, $\partial w/\partial n = 0$, $v=0$) at the spanwise sides. Uniform wind flow with a speed of 5.4 m s^{-1} was set at the inlet ($p = 0$, $u=5.4$ m s^{-1}, $v=0$, $w=0$). At the end of the tunnel outlet boundary condition ($\partial p/\partial n = 0$, $\partial u/\partial n = 0$, $\partial v/\partial n = 0$,..) is applied. Non-slip condition ($u=0$, $v=0$, $w=0$, $\partial p/\partial n = 0$) for velocity was used at the bottom surface.

Throughout the whole domain the vertical grid distribution does not change. The vertical grid size in the grass has a uniform size of 0.5 mm. Starting from the top of the grass the vertical grid size grows at a ratio of 1.15. With the intent to quantitatively investigate the turbulent features near the target region, two nested grids were used as presented in Fig. 8 where the area colored by dark gray shows the fine grid region. The fine grid domain extends over (L_x, L_y, L_z)=(0.82 m, 0.2 m, 0.9 m) in the x(streamwise), y (spanwise) and z(vertical) directions. The length of the upstream fine grid region, 0.5 m, is larger than that of the downstream one, 0.32 m, in order to provide enough upstream space to prevent the influence from the change of the grid size to be transported into the region of concern. By changing the length of the upstream and downstream fine grid region, 0.5 m upstream and 0.32 m

downstream has been found as the optimized ones. As could be found from the following discussion about the fluid visualizations, these two lengths are large enough to absorb the perturbations from the change of the grid at the beginning and the end of the fine grid domain. In the fine grid region, the horizontal grid shape is square. The horizontal (x–y plane) resolutions of 5.0 mm, 4.0 mm, 2.0 mm, 1.0 mm have been examined. At last the meshes with horizontal resolution of 2.0 mm and 1.0 mm showed almost the same results, indicating that the grid independence achieves when the horizontal grid size is 1.0 mm. Therefore, in the fine grid region horizontal grid size of 1.0 mm was used. In between the rough grid region, as shown by the white color, and the fine grid region, as shown by the dark gray color, a buffer zone, as shown by the light gray color in Fig. 8, the horizontal grid size increasing from 1.0 mm to 5.0 mm was used. Horizontal grid shape in the buffer zone is quadrangle and has a growing factor of 1.2. In the rough grid region, the horizontal grid shape is square and the grid size is 5.0 mm which is same as the height of the vegetation canopy. This grid nesting procedure used here allows us to use a wide enough computational domain to limit the impact of the symmetry conditions at the sides and to simulate the flow with an acceptable computational time. The cost would be much higher if only the fine resolution is used. The choice of the size and resolution of our nested domains results from a compromise between constraints related to the available computational time and the factor that the domain should be large enough to represent the largest eddies and fine enough to represent the smallest eddies of interest. In Fig. 8 white dashed line shows the area covered by the 3-D hill which will be discussed later. The total grid number is 31.5 million.

3.2.2. Numerical results

It is interesting to look at the instantaneous flow fields across the nested grids. Vorticities in y direction, $\partial w/\partial x - \partial u/\partial z$, on the slice of $y=0$ at a given time $t=8$ s, are plotted in Fig. 9. As expected, turbulent structures appear much more detailed in the fine grid domain than the coarse grid domain. Some damping effects are visible at the inflow boundary of the fine grid domain. At the
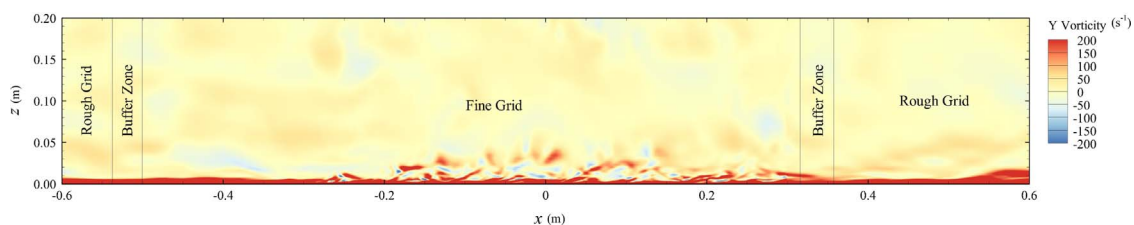
Fig. 9. Turbulence features of the flow over flat terrain covered by vegetation on the vertical slice crossing $y=0$.
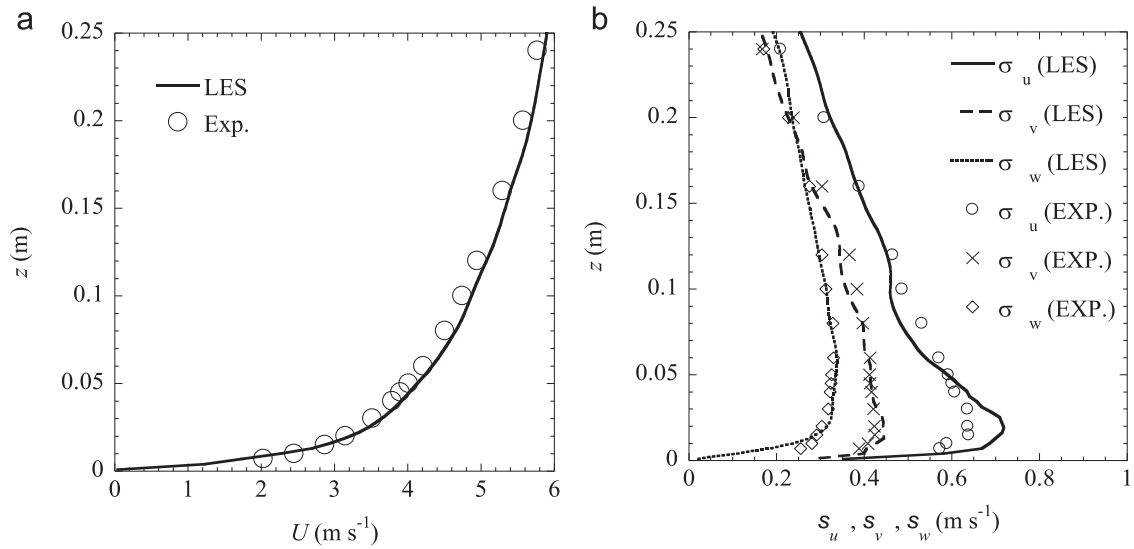
Fig. 10. Vertical profiles of (a) normalized mean velocity and (b) normalized turbulence fluctuations of the flow over flat terrain covered by vegetation at the site of $x=0$, $y=0$.
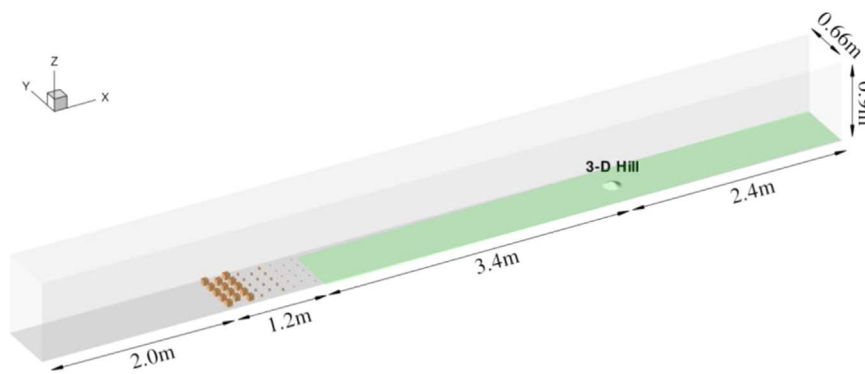
Fig. 11. Configuration of numerical model simulating the 3-D hill covered by vegetation canopy.
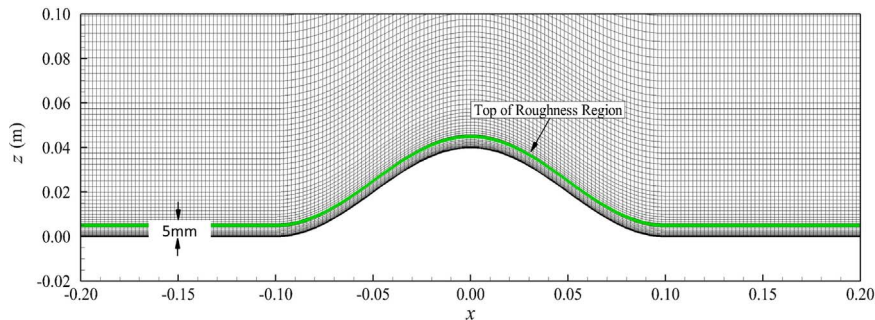
Fig. 12. Distributions of the mesh on the vertical slice crossing the center of the 3-D hill covered by vegetation canopy.
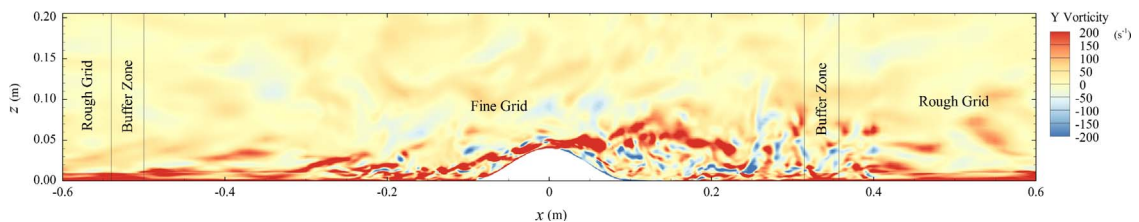
Fig. 13. Turbulence features of the flow over a 3-D hill covered by vegetation on the vertical slice crossing $y=0$.

location of $x=0$ the flow becomes stable and the perturbations from inlet of the fine grid domain become weak enough. It could also be found the influence from the outlet of the fine grid domain into the region of concern has been avoided which means the fine grid space with length of 3.2 m after the origin point is large enough.

The vertical profiles of the normalized mean and standard
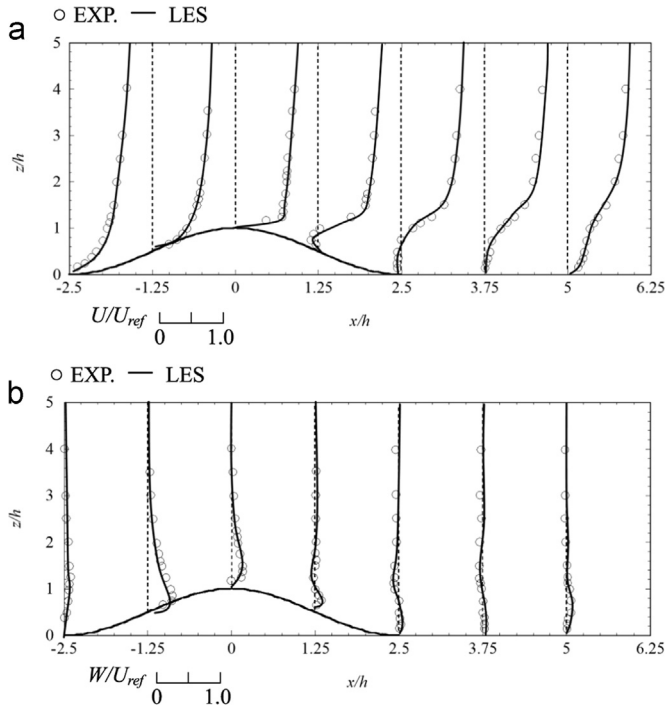
Fig. 14. Profiles of the normalized mean velocities of the flow over 3-D hill covered by vegetation canopy, (a) streamwise component and (b) vertical component on the vertical slice crossing $y=0$.

deviation of the streamwise component in the undisturbed boundary layer are shown in Fig. 10, where the referred velocity, U_{ref}, was decided as the wind speed outside of the boundary layer, 5.8 m s^{-1}. The numerical results show fairly good agreement with the measurements, validating the accuracy of this numerical wind tunnel. The vertical profiles of mean velocities as well as three components of fluctuations at the locations of $x=-0.25$ m, $y=0$ and $x=0.25$ m, $y=0$ are also extracted and compared with those at $x=0$, $y=0$. The comparisons between them are in good agreement (not shown in the figure), implying a fully developed and stable boundary layer.

3.3. 3-D hill covered by vegetation canopy

In this section we want to further validate this method by the same numerical wind tunnel used above but a 3-D hill topography is introduced on the bottom.

3.3.1. Simulation setup

The 3-D hill has the shape $z(x,y)=h\cos^2\pi(x^2+y^2)^{1/2}/2L$ with $h=40$ mm and $L=100$ mm. The maximum slope was thus about 32°. Except the 3-D hill introduced on the bottom of the numerical wind tunnel, see Fig. 11, all of the other configuration parameters are identical with the above discussion about the flat terrain. The height of the vegetation is also 5 mm. The boundary conditions, the grid distributions are same as those in Section 3.2. σ grid is applied to change the locations of the vertical grid nodes, which means keeping the ratio of the vertical sizes of adjacent grids unchanged. Fig. 12 shows the side view of the 3-D hill and the vertical mesh distribution.

3.3.2. Numerical results

Vorticities in y direction, $\partial w/\partial x - \partial u/\partial z$, on the slice of $y=0$ at a given time $t=8$ s, are plotted in Fig. 13. When we put a 3-D hill on the bottom of the numerical wind tunnel, the flow pattern in downstream regions shows quite different characteristics
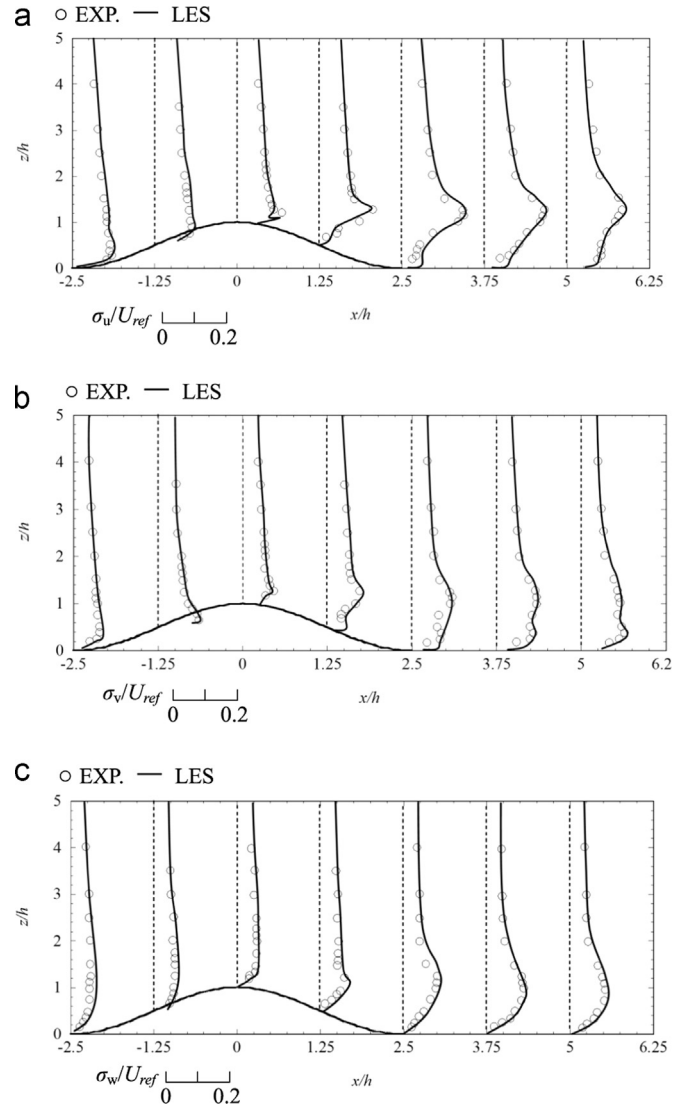
Fig. 15. Profiles of the normalized turbulence fluctuations of the flow over a 3-D hill covered by vegetation canopy, (a) streamwise component, (b) spanwise component and (c) vertical component on the vertical slice crossing $y=0$.

compared with that in the upstream region. The effects of the 3-D hill on the instantaneous wind generate a series of vortices clearly behind the summit where the contrast between colors becomes larger compared with that upstream of the hill, indicating a more intense turbulence in the wake. Same as the flat terrain case, the turbulence has fully developed at the foot of upwind side of the 3-D hill and the perturbations from inlet of the fine grid domain become weak enough. The influence from the outlet of the fine grid domain into the region of concern has been avoided as well.

Vertical profiles of streamwise and vertical mean velocities at several downstream locations from $x=-2.5h$ to $x=6.25h$ with a step size of $1.25h$ for the 3-D hill are shown in Fig. 14 (a) and (b) respectively. The profiles are normalized by the mean velocity, U_{ref}, outside of the boundary layer in the freestream flow, which is 5.8 m s^{-1}. On the whole, the numerical results provide acceptable agreement with those in experiment for the mean velocity components.

The vertical profiles of normalized fluctuations by U_{ref} are plotted as shown in Fig. 15, where Fig. 15(a) is for the streamwise component, σ_u, Fig. 15(b) is for the spanwise component, σ_v, and Fig. 15(c) is for the vertical component, σ_w. At the foot of upwind side of the 3-D hill, the profiles of turbulent fluctuations give good
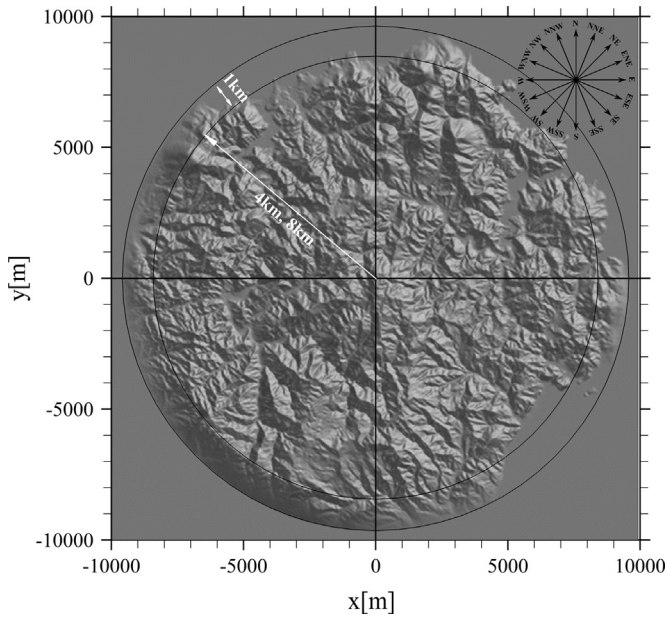
Fig. 16. Topography map of the terrain near Taikoyama hill, Kyoto, Japan.

agreement between the numerical prediction and the experimental data. At the lee side of the hill the simulated results are comparable with the experimental data as a whole, however, in the range from $x=2.5h$ to $x=3.75h$, the LES results slightly overestimate the experiment. The locations of the separated shear layer where the peaks of σ_u occur are very well reproduced and the shapes of the profiles are almost same. The height of shear layer increases from $1h$ at $x=0h$ to $1.4\ h$ at $x=5h$. The influence by

the hill covers a long distance. This is the indication that in order to well reproduce the flow over a real terrain the tall hills near the measurement points should be included in the model.

The satisfactory agreement with the experimental data for the mean wind velocities and the turbulence fluctuations validates that the method adopted in the present research is applicable for the vegetation covered curved terrain. In the following case we will apply this technique to simulate the real forested topography.

3.4. Real complex terrain covered with vegetation canopy

One wind turbine accident occurred in Taikoyama Hill near Kyoto, Japan, as have been reported by Kyoto Prefecture (2013). Extensive measurement data are available in this wind farm, therefore the very complex topography around Taikoyama Hill, as shown in Fig. 16, was chosen to do examinations.

3.4.1. Simulation setup

Two 1:2000 topography models with radius $R=4$ km and 8 km were built to examine the terrain size effects. The origin of this topography located at the wind measurement Mast in Taikoyama wind farm. The outer ring of this terrain with width of 1 km was used to smooth the surrounding area through function:

$$z_m(x, y) = \begin{cases} 0 & 1000 + R \le \sqrt{x^2 + y^2} \\ z(x, y) \cdot \left[1 - \left(\sqrt{x^2 + y^2} - R \right)/1000 \right] & R \le \sqrt{x^2 + y^2} \le 1000 + R \\ z(x, y) & 0 \le \sqrt{x^2 + y^2} \le R \end{cases} \tag{12}$$

in which the unit is meter and z_m is the height after modification. A domain with dimensions of 30 km × 30 km × 6 km (streamwise direction, spanwise direction and vertical direction) was used, see Fig. 17(a). Roughness blocks with height of 60 m (3 cm in scale)
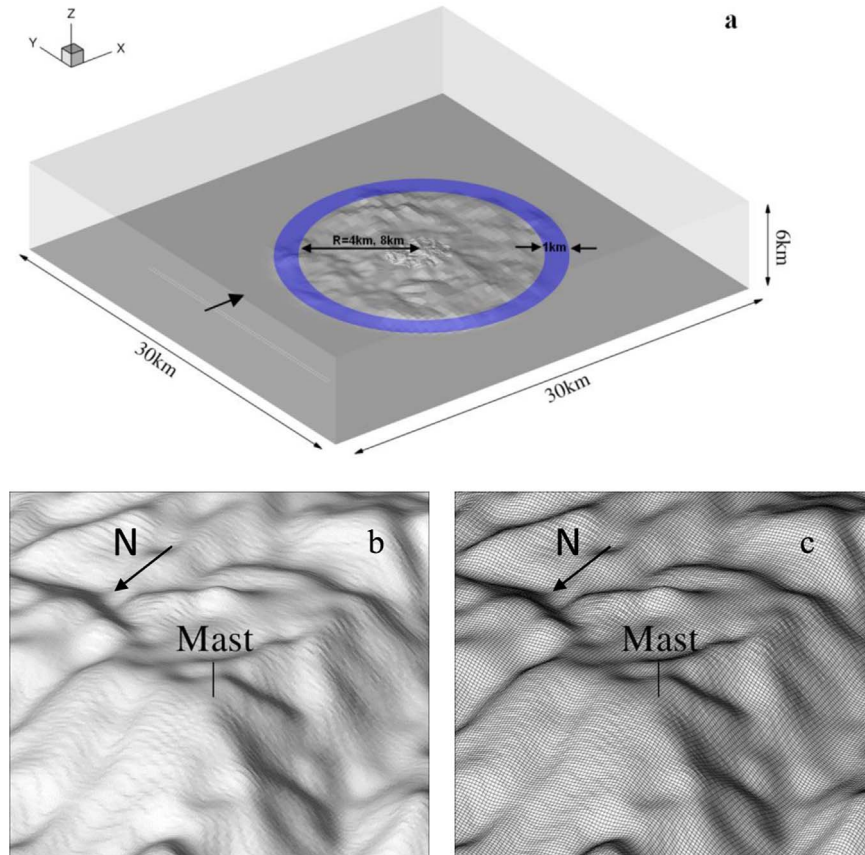
Fig. 17. Configuration of numerical model simulating Taikoyama hill, (a) global view of model; (b) terrain near the Mast; and (c) mesh near the Mast.
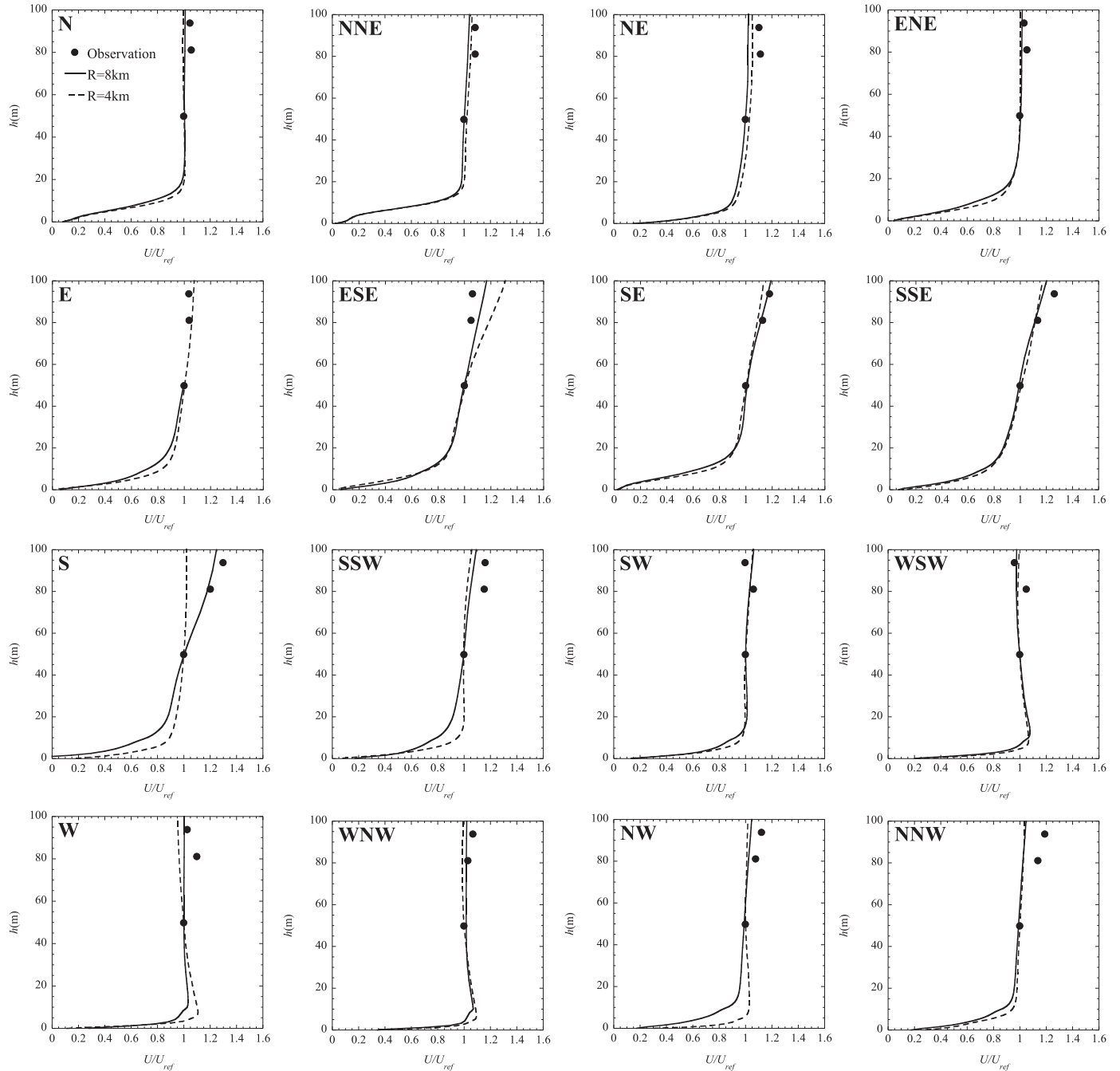
Fig. 18. Profiles of the normalized mean streamwise velocity under sixteen wind directions for the case of Taikoyama hill.

were located 12 km upstream from the Mast. Fine grid domain is horizontally a square centered at the Mast with side length of 1.5 km (0.75 m in scale). Resolution of 6 m (3 mm in scale) was applied in the fine grid domain as shown in Fig. 17(c). With the consideration that the averaged height of forest is about 15 m as reported by Næsset (1997), this height was used for the canopy height and the number of canopy layers is 10. In the numerical wind tunnel in scale the terrain was geometrically simulated and the forest was modeled by the artificial grass as has been discussed in the above sections about the flow over flat terrain and 3-D hill. The same occupancy rate γ_0 and the leaf thickness l_0 were applied in this simulation. From the roughness blocks to the fine grid region the horizontal grid size is 15 m (7.5 mm in scale) which is

same as the height of the roughness canopy to capture the turbulent characteristics with sufficient accuracy. From the ground surface to the upper boundary, the grid spacing was gradually stretched from 1 m (0.5 mm in scale) to 540 m (270 mm) with maximum stretching ratio equaling to 1.2. In the vertical direction σ grid method was applied to fit the hill shape. The total mesh number is 2.21×10^7.

As boundary conditions, a stress-free condition ($\partial u/\partial n = 0$, $\partial v/\partial n = 0$, $w=0$) was used at the top of the domain and a symmetry condition ($\partial u/\partial n = 0$, $\partial w/\partial n = 0$, $v=0$) at the spanwise sides. Uniform wind flow with a speed of 5.0 m s^{-1} was set at the inlet ($p = 0$, $u=5.0$ m s^{-1}, $v=0$, $w=0$). At the end of the tunnel outlet boundary condition ($\partial p/\partial n = 0$, $\partial u/\partial n = 0$, $\partial v/\partial n = 0$, $\partial w/\partial n = 0$) is applied. Non-slip condition ($u=0$, $v=0$, $w=0$, $\partial p/\partial n = 0$) for
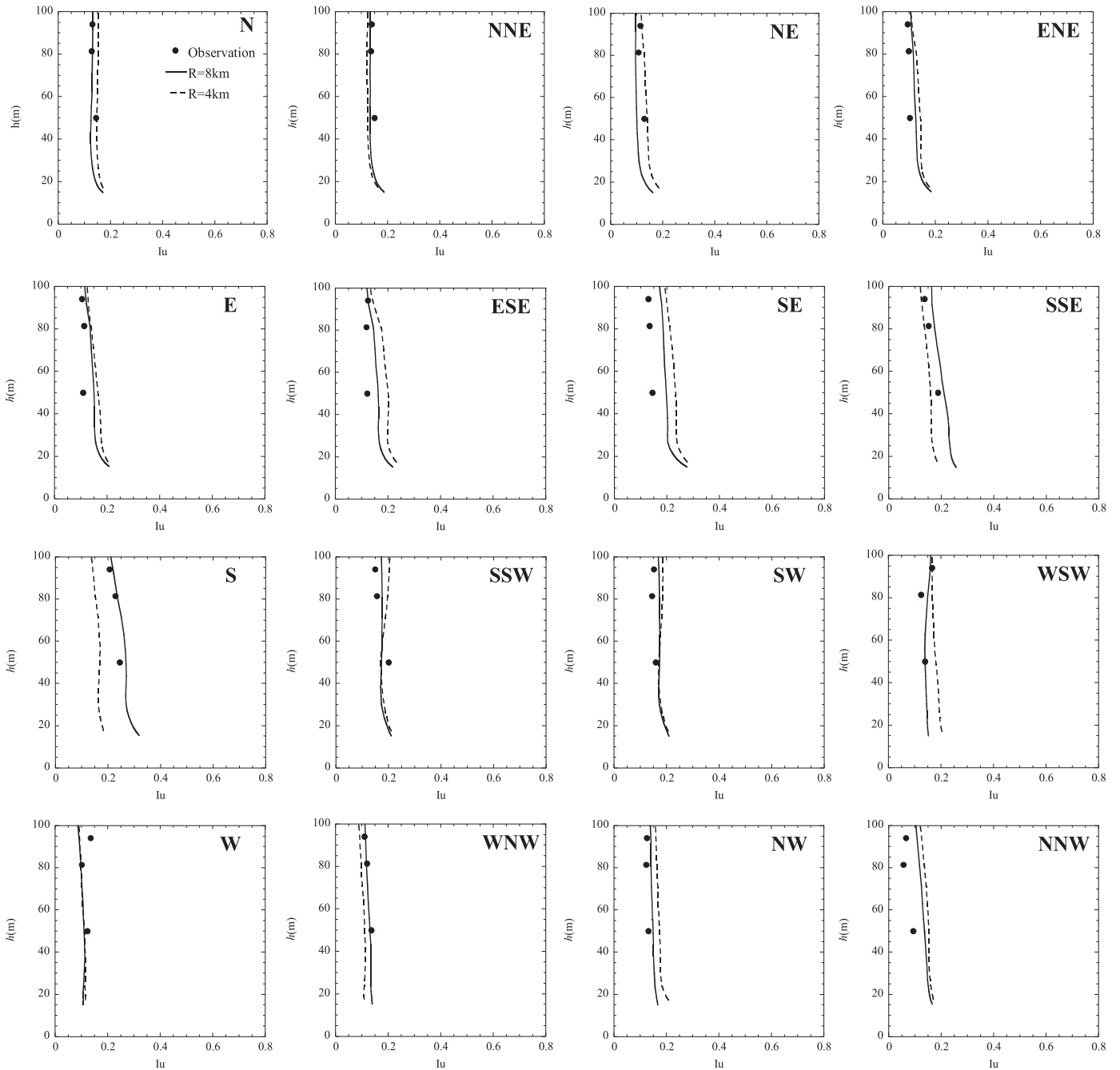
Fig. 19. Profiles of the turbulence intensity at sixteen wind directions for the case of Taikoyama hill.

velocity was used at the bottom surface. Sixteen wind directions, as shown in Fig. 16, were simulated. For each wind direction, the numerical wind tunnel was not changed. What we did was like the turn table in wind tunnel, which means the coordinates of the terrain were rotated when the wind direction was changed.

3.4.2. Numerical results

Fig. 18 shows the comparison of mean streamwise velocity at Mast, normalized by U_{ref} which is the mean streamwise velocity at $z' = 50$ m (25 mm in scale), where z' is the height relative to the ground, between observation and simulated results from the two models. The steep-up of the wind velocity near the ground could be found when the wind is from the directions close to the west. At the directions of WSW, W, and WNW, the profiles of the mean streamwise velocity are close to that at the summit of the 3-D hill

as shown in Fig. 14(a). Whereas, when the wind is from the direction close to south, such as SE, SSE, and S, the profiles of the mean streamwise velocity are close to that at the far wake of the 3-D hill, and the most important thing is that only the model with large topography region ($R = 8$ km) provides satisfactory prediction when the wind is from south. The turbulence intensities of the streamwise component, $I_u = \sigma_u/U$, at the Mast from numerical simulations of the two models are also compared with those of observations, as shown in Fig. 19, from which it is found that when the wind is from south the small topography model gives very large error, while fairly good agreement is achieved by large model. For the other wind directions, these two models give similar results. In order to explain why only the large topography can reproduce the observed data when the wind is from south, the streamwise velocity contours on the vertical crossing section when
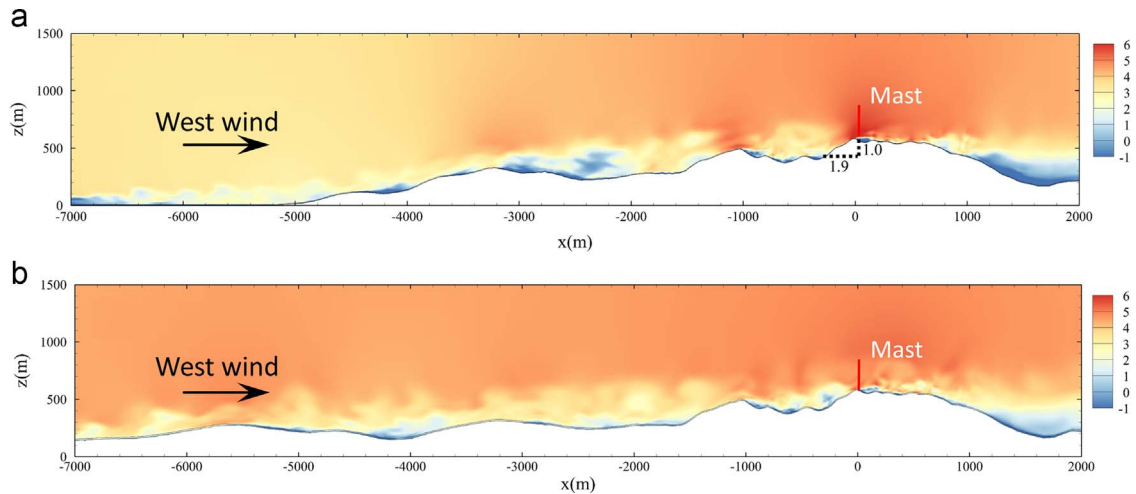
Fig. 20. Instantaneous flow fields visualized by streamwise velocity over the terrain with R equals to (a) 4 km; (b) 8 km; when the wind is from west.
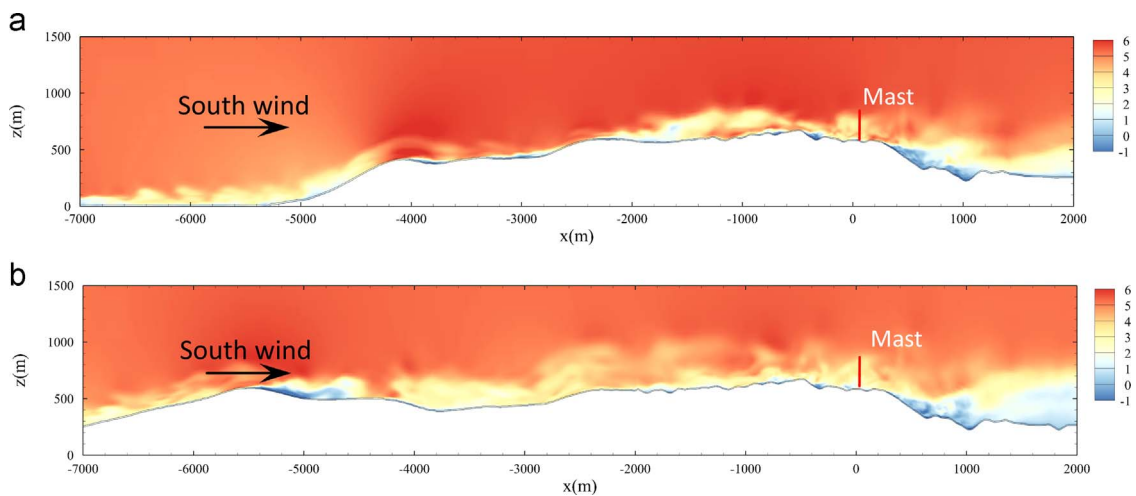
Fig. 21. Instantaneous flow fields visualized by streamwise velocity over the terrain with R equals to (a) 4 km; (b) 8 km; when the wind is from south.

the wind is from south are plotted in Fig. 21. In order to do comparison, the flow fields of another case under the west wind are also plotted, as shown in Fig. 20. Comparing Fig. 20 (a) and (b) it could be found that even the region exceeding $R=4$ km is smoothed, where there is no upstream tall hills, the flow pattern especially the thickness of the boundary layer is not affected much, which is the answer why both small and large topography models could predict the flow accurately when the wind is from west. Moreover, the upstream terrain of the Mast is very sharp with a maximum slope of 1:1.9, as plotted in Fig. 20(a). That is why the profile of the mean streamwise velocity shows the similar shape of that at the summit of the 3-D hill. If the wind comes from south, a hill with altitude about 550 m could be found 5.5 km upstream of the Mast. When the small topography model is used, this tall hill will be cut, and from the comparison between Fig. 21(a) and (b), we can clearly identify that the flow patterns are very different. The height under which the flow shows large fluctuations is larger when the topography is large. It means that the boundary layer simulated by large topography model is much thicker than that by small topography model,

indicating that the disturbance due to the upstream tall hill could still influence the flow in the far wake region. This is the reason why only the large topography can reproduce the observed data when the wind is from south. The above simulations only consider the ideal homogeneous roughness canopy. In the real situation the roughness density will be different in different locations. Therefore, in the future, we will carry out the simulation using the data from Geographic Information System (GIS) to study the flow fields over real complex terrain.

4. Conclusions

In this study the turbulent flow fields over, (a) flat terrain covered by roughness blocks, (b) flat terrain covered by vegetation canopy, (c) 3-D hill covered by vegetation canopy and (d) real forested complex terrain, are numerically predicted by large eddy simulations. Firstly, the roughness canopy model together with the LES model applied is capable of simulating velocities fields over different types of terrain. The mean velocity distributions,

turbulent fluctuations, and the fluctuations ratios are examined and show good agreement with those measured in experiments. Secondly, in order to successfully reproduce the flow fields over roughness canopy the horizontal grid size should be at least as large as height of the roughness canopy. Lastly, the simulations of a real terrain by two models with difference topography sizes suggest that the small size 4 km model cannot include the tall hill that the south wind quickly meets and this actually changes the entire flow field in the south wind case. The wake effect from the upstream tall hill is very large and in order to provide a good prediction that tall hill should be included in the simulated region.

Acknowledgments

References

Cao, S., Tamura, T., 2006. Experimental study on roughness effects on turbulent boundary layer flow over a two-dimensional steep hill. J. Wind Eng. Ind. Aerodyn. 94, 1–19.

Cao, S., Tamura, T., 2007. Effects of roughness blocks on atmospheric boundary layer flow over a two-dimensional low hill with/without sudden roughness change. J. Wind Eng. Ind. Aerodyn. 95, 679–695.

Cao, S., Wang, T., Ge, Y., Tamura, Y., 2012. Numerical study on turbulent boundary layers over two-dimensional hills – effects of surface roughness and slope. J. Wind Eng. Ind. Aerodyn. 104–106, p342–p349.

Castro, F., Palma, J., Lopes, A., 2003. Simulation of the Askervein flow. Part 1: reynolds averaged Navier–Stokes equations (k–ε turbulence model). Bound.-Layer Meteorol. 107, 501–503.

Dupont, S., Brunet, Y., Finnigan, J., 2008. Large-eddy simulation of turbulent flow over a forested hill: validation and coherent structure identification. Q. J. R. Meteorol. Soc. 134, 1911–1929.

Diebold, M., Higgins, C., Fang, J., Bechmann, A., Parlange, M., 2013. Flow over hills: a large-eddy simulation of the bolund case. Bound.-Layer Meteorol. 148, 177–194.

Enoki, K., Ishihara, T., 2012. A Generalized canopy model and its application to the prediction of urban wind climate. J. Jpn. Soc. Civil Eng. A1 68, 28–47 (in Japanese).

Fluent Inc, 2006. Fluent 6.3 User's Guide. Fluent Inc., Lebanon.

Finnigan, J., Raupach, E., Bradley, E., Aldis, G., 1990. A wind tunnel study of turbulent flow over a two-dimensional ridge. Bound.-Layer Meteorol. 50, 277–317.

Ferziger, J., Peric, M., 2002. Computational Method for Fluid Dynamics, third ed. Springer.

Ishihara, T., Hibi, K., 1998. An experimental study of turbulent boundary layer over steep hills. In: Proceedings of the 15th National Symposium on Wind Engineering, pp. 61–66 (in Japanese).

Ishihara, T., Fujino, Y., Hibi, K., 2001. A wind tunnel study of separated flow over a two-dimensional ridge and a circular hill. J. Wind Eng. 89, 573–576.

Kaimal, J.C., Finnigan, J.J., 1994. Atmospheric Boundary Layer Flows: Their Structure and Measurements. Oxford University Press, New York.

Kim, H., Patel, V., Lee, C., 2000. Numerical simulation of wind flow over hilly terrain. J. Wind Eng. Ind. Aerodyn. 87, 45–60.

Kyoto Prefecture, 2013. 京都府太鼓山風力発電所�号機ナセル落下事故報告 (in Japanese).

Liu, Z., Ishihara, T., Tanaka, T., He, X., 2016. LES study of turbulent flow fields over a smooth 3-D hill and a smooth 2-D ridge. J. Wind Eng. Ind. Aerodyn. 153, 1–12.

Lopes, A., Palma, J., Castro, F., 2007. Simulation of the Askervein flow. Part 2: large-eddy simulations. Bound.-Layer Meteorol. 125, 85–108.

Lun, Y., Mochida, A., Murakami, S., 2003. Numerical simulation of flow over topographic features by revised k–ε models. J. Wind Eng. Ind. Aerodyn. 91, 231–245.

Maruyama, T., 1993. Optimization of roughness parameters for staggered arrayed cubic blocks using experimental data. J. Wind Eng. Ind. Aerodyn. 46 (47), 165–171.

Mason, P.J., Thomson, D.J., 1987. Large-eddy simulations of the neutral-static-stability planetary boundary layer. Q. J. R. Meteorol. Soc. 113, 413–443.

Næsset, E., 1997. Determination of mean tree height of forest stands using airborne laser scanner data. J. Photogramm. Remote Sens. 52, 49–56.

Tamura, T., Cao, S., Okuno, A., 2007. LES study of turbulent boundary layer over a smooth and a rough 2D hill model. Flow Turbul. Combust. 79, 405–432.

Yamaguchi, A., Ishihara, T., Fujino, Y., 2003. Experimental study of the wind flow in a coastal region of Japan. J. Wind Eng. Ind. Aerodyn. 91, 247–264.